Water Research 186 (2020) 116388

Contents lists available at ScienceDirect

Water Research

journal homepage: www.elsevier.com/locate/watres

Rainfall and conduit drainage combine to accelerate nitrate loss from a karst agroecosystem: Insights from stable isotope tracing and high-frequency nitrate sensing

Fu-Jun Yue[a,b,c], Si-Liang Li[a,c,*], Susan Waldron[b], Zhong-Jun Wang[d], David M. Oliver[e], Xi Chen[a,c], Cong-Qiang Liu[a,c]

[a] Institute of Surface-Earth System Science, School of Earth System Science, Tianjin University, Tianjin 300072, China
[b] School of Geographical and Earth Sciences, University of Glasgow, Glasgow G12 8QQ, United Kingdom
[c] Tianjin Key Laboratory of Earth Critical Zone Science and Sustainable Development in Bohai Rim, Tianjin University, Tianjin 300072, China
[d] State Key Laboratory of Environmental Geochemistry, Institute of Geochemistry, Chinese Academy of Sciences, Guiyang 550081, China
[e] Biological & Environmental Sciences, Faculty of Natural Sciences, University of Stirling, Stirling FK9 4LA, United Kingdom

ARTICLE INFO

Article history:
Received 26 May 2020
Revised 29 July 2020
Accepted 2 September 2020
Available online 3 September 2020

Keywords:
Nitrate
Dual isotope
High-frequency
Rainfall events
Karst critical zone

ABSTRACT

Understanding where nitrate is mobilized from and under what conditions is required to reduce nitrate loss and protect water quality. Low frequency sampling may inadequately capture hydrological and biogeochemical processes that will influence nitrate behavior. We used high-frequency isotope sampling and in-situ nitrate sensing to explore nitrate export and transformation in a karst critical zone. Nitrate was mobilised during light rainfall, and transferred from soil layers to the karst matrix, where some nitrate was retained and denitrified. Nitrate isotopic composition changed rapidly during the rising limb of events and slowly during the falling limb. The main nitrate source was synthetic fertiliser (up to 80% during event flow), transported by conduit flow following high rainfall events, and this contribution increased significantly as discharge increased. Soil organic nitrogen contribution remained constant indicating at baseflow this is the primary source. Isotope source appointment of nitrate export revealed that synthetic fertilizer accounted for more than half of the total nitrate export, which is double that of the secondary source (soil organic nitrogen), providing valuable information to inform catchment management to reduce nitrate losses and fluvial loading. Careful land management and fertilizer use are necessary to avoid nitrate pollution in the karst agroecosystem, for example by timing fertilizer applications to allow for plant uptake of nitrate before rainfall can flush it from the soils into the karst and ultimately into catchment drainage.

1. Introduction

The critical zone (CZ) is the near-surface layer that ranges from the top of plants through to the base of the groundwater zone; it serves as the main region within which biogeochemical processes interact to sustain terrestrial ecosystems (Banwart et al., 2013; Brantley et al., 2006). As an essential nutrient, nitrogen (N) has a critical influence on organisms within the CZ. Understanding the fate and behavior of N in the CZ is important to manage potential N losses from the terrestrial environment. As one of the major pathways for active N to enter the ecosystem, application of synthetic and organic N fertilisers to agricultural land is essential to support food production for a growing population (Gu et al., 2015; Zhang et al., 2015). However, when applied in excess of crop requirements, N can transfer from land to water and result in high concentrations of nitrate-N (NO_3^-–N) in aquatic environments of the CZ (Cui et al., 2013).

Karst geology accounts for 20% of the ice-free global terrestrial environment and supports water sources for approximately one quarter of the world population (Ford and Williams, 2013; Sullivan et al., 2019). The hydrology of karst is complex due to the multiple porosities of the geology which facilitate conduit, fracture and matrix flows and results in unique dual hydrological flows (e.g. rapid flow by conduit porosity and diffusion flow via fractures and the karst matrix), which may distinguish it from other kinds of CZ (Ford et al., 2019; Kordilla et al., 2012). Hydrological response to rainfall events in karst areas is often quick, and rapid exchange between surface and underground streams promotes the transfer of

* Corresponding author.
E-mail address: siliang.li@tju.edu.cn (S.-L. Li).

https://doi.org/10.1016/j.watres.2020.116388
0043-1354/

pollutants, e.g. nitrate, from agricultural to aquatic environments (Epting et al., 2018; Jiang et al., 2009). However, low frequency sampling, e.g. monthly or even weekly, fails to fully capture hydrological responses, and associated physical, chemical and biogeochemical processes, typical of karst environments (Huebsch et al., 2014; Pu et al., 2011; Yang et al., 2019).

Improved knowledge of nitrate source characteristics is needed, and high-resolution understanding of source contribution dynamics is also required to understand where and when nitrate is exported from nitrate rich or poor zones in the karst critical zone (KCZ) and how land use influences the KCZ - thus helping to identify risk of elevated nitrate export periods (Hartmann et al., 2014; Huebsch et al., 2014; Sebestyen et al., 2019). For example, high-resolution monitoring of fluvial nitrate export in karst in Southwestern China showed that strong seasonal export was controlled by land use: intense nitrate export coincided with summer crop agricultural practices, particularly rice cultivation when water is pumped from sinkholes or wells for seeding and transplanting (Yue et al., 2019). Further nitrate export was controlled by changes in catchment hydrology, particularly during intensive rainfall in the wet season (Yue et al., 2019) and here the transition from dry to wet conditions could offer particular insight.

Understanding where nitrate comes from is not possible from monitoring only concentration profiles in receiving waters due to loss of material from nitrate reprocessing, source mixing, and variation in hydrological flow pathways (Hu et al., 2019; Huebsch et al., 2014; Jarvie et al., 2018). Isotopic approaches have been used widely in landscape studies over the past few decades to identify nitrate sources and transformations based on the distinct isotopic compositions of sources and changes to that during reprocessing (Gooddy et al., 2016; Jiang et al., 2009; Musgrove et al., 2016; Wong et al., 2012). High frequency nitrate isotopic composition during high risk periods (e.g. rainfall events), may provide insightful understanding of nitrate biogeochemistry, (Hu et al., 2019; Husic et al., 2019a, 2020), but this approach is not common. By coupling this modeling approach with an understanding of the system hydrology (Parnell et al., 2010), the dynamic contribution from each source can be clearly profiled at high resolution to help identify nitrate mobilization within a catchment.

To elucidate nitrate dynamics during the more intense nitrate export periods, important for informing global karst catchment management, we coupled high-resolution nitrate dual isotopes profiling with nitrate sensor time series to 1) understand how different sources of nitrate contribute quantitatively to export and 2) determine how this changes with differences in hydrology and land management practices. We hypothesised that the controls on more intense nitrate export will be spatial storage of nitrate, and the extent to which these storage zones are connected with hydrological flow pathways in the karst.

2. Material and methods

2.1. Study area

This research took place in Chenqi (CHQ), a headwater catchment of the Houzhai Karst Critical Zone Observatory (KCZO), with a drainage area of 1.25 km^2 and elevation of 1316 – 1500 m above sea level (Fig. 1a). It is located in a subtropical monsoonal climate zone with annual precipitation between November 2016 and October 2017 (the research period) of 1217 mm, which was slightly less than the average precipitation for a typical year (1246 $\pm$ 315 mm) (Yue et al., 2018). Approximately 86% of the annual precipitation occurs in the wet season (May to October), particularly in June and August for 2017 (Yue et al., 2019). Geological strata in this headwater catchment include dolostone, pure and thick limestone of the Guanling Formation of the Middle Triassic, marlite, and Quaternary soil (Fig. 1a) (Chen et al., 2018). The typical geomorphology in the study area is peak clusters with many valleys. Therefore, soil thickness on hillslopes is thinner than in the valley floor where soil deposition originating from the surrounding hillslope occurs (Green et al., 2019). The soil thickness is 20 – 50 cm with clay content of 24 – 32.5 g/100 g, total nitrogen of 1.24 –13.02 g/kg and organic matter content of 15.95 –192.9 g/kg (Luo et al., 2019; Peng and Wang, 2012).

Land use includes farmland (16.6% including 13.8% for dry land and 2.8% for paddy field), natural vegetation (82.8%) and other land cover, e.g. developed areas (0.3%) and bare rock (0.3%) (Yue et al., 2019). The agricultural fields are mainly located on hillslopes for dry land and in valleys for paddy field and vegetable cultivation (Fig. 1b). High intensity fertilizer application to land occurs from May to July for summer crops. Synthetic and organic fertilizers are generally used, with organic sources more commonly used to fertilize paddy fields (Yue et al., 2018).

2.2. Sampling and analyses

Nitrate concentration ($[NO_3^-–N]$) and water discharge (Q) at the CHQ catchment outlet was measured using an in-situ sensor approach (Chen et al., 2018; Yue et al., 2020). To avoid optical sensor interference from turbid event flow waters in the karst systems, nitrate ion-selective electrodes (NISE) sensors were used in the study area. The NISE sensor can measure and compensate for chloride present in the water to eliminate cross sensitivity between nitrate and chloride. In addition, discrete samples for validation of sensor estimate of $[NO_3^-–N]$ were collected, and immediately filtered for analysis. Linear relationship calibration between sensor $[NO_3^-–N]$ and laboratory measured $[NO_3^-–N]$ from discrete samples was used and the uncertainty (μ_C) of calibration was evaluated - which ranged from 0.06 to 0.64 mg/L over the 18 months monitoring period (further details in Yue et al. (2020)). To help understand the dynamics of solute and water, temperature (T), conductivity (EC), and dissolved oxygen (DO) were monitored using a multi-parameter sonde (Aqua Troll 600, In Situ Inc., Fort Collins, USA).

The most dynamic exports were previously observed during the transition from dry aquifer conditions to wet conditions, i.e. from May to middle of June in 2016 (Yue et al., 2019). Thus, high frequency sampling by autosamplers (TC-8000E-II, China) with different time intervals was implemented at Chenqi spring outlet during rainfall events between 14th May and 3rd July 2017 (Fig. 1b). The time interval between samples was typically one hour during event flow. As event flow subsided the time interval between samples was increased, e.g. a transition to two, four and six hours between samples with the continued decrease in Q. Up to 24 bottles could be stored in dark conditions within the autosampler unit allowing daily collection. All samples were filtered immediately after collection in the laboratory using 0.45 μm cellulose acetate filters before storing at 4 °C to await isotopic analysis. The nitrate and hydrochemistry sensor data were used to assess variability in hydrochemistry and decide which collected samples would be analysed for $\delta^{15}N$ and $\delta^{18}O$ of the NO_3^-. Thus, 347 samples (63% of total samples) were selected for nitrate isotope analysis within 1 month. To help identify nitrate sources from synthetic fertilisers and manure, $[Cl^-]$ was also measured using a Dionex ion chromatography (Dionex Corp., Sunnyvale, CA, USA) with a precision of +/- 5%.

The fluvial filtrate was analyzed for $\delta^{15}N$ and $\delta^{18}O$ of NO_3^- by the denitrifier method (McIlvin and Casciotti, 2011) and an Isoprime Continuous Flow Isotope Ratio Mass Spectrometer (CF-IRMS) equipped with a Gilson GX271 autosampler and a Trace Gas Preconcentrator unit (IsoPrime, GV, UK) at the State Key Laboratory of Environment Geochemistry, Chinese Academy of Science. Four international nitrate (USGS-32, USGS-34, USGS-35 and IAEA-N3) and

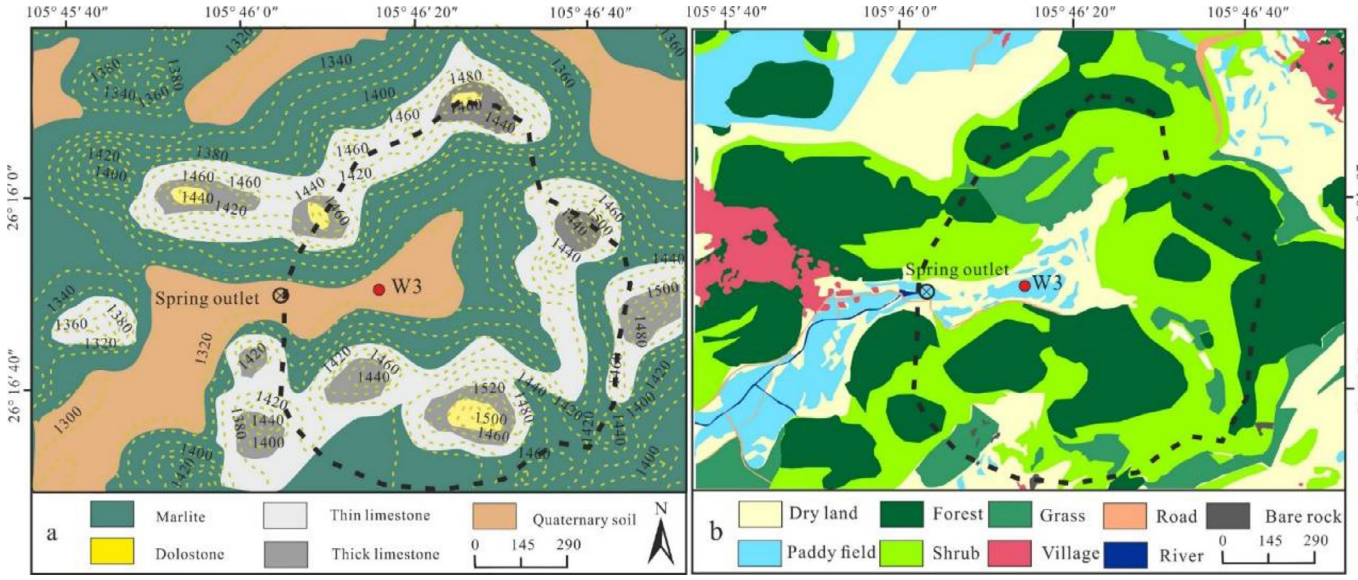

Fig. 1. Chenqi catchment (a) geomorphology, modified from Chen et al. (2018) and (b) land use in the Chenqi catchment (Yue et al., 2019). The yellow and black dashed lines represent elevation contours and catchment boundary, respectively.

two laboratory reference materials were used for the calibration. The analytical precision for the replicated samples was 0.3‰ for $\delta^{15}N$ and 0.5‰ for $\delta^{18}O$ of nitrate ($n = 5$).

2.3. Water yield and nitrate yield calculation

The water volume (m^3) and nitrate loading (kg) during each period was calculated using the following equations, respectively:

$$\text{Water volume} = \sum_{i=1}^{N} Q_i \times 60 \times 15 \quad (1)$$

$$\text{Nitrate loading} = k \times \sum_{i=1}^{N} \frac{(Ci \times Qi \times 60 \times 15)}{1000} \quad (2)$$

where C_i and Q_i are $[NO_3^-–N]$ (mg/L) and discharge (m^3/s) with time interval of 15 mins. Constant k is 10^{-6} to convert units from mg to kg. N is the total number of measurements during the monitoring period with time interval of 15 mins. Water yield (mm/day) and nitrate yield (kg/km^2/day) were calculated using water volume and $[NO_3^-–N]$ loading.

$$\text{Water yield} = \left(\frac{\text{water volume}}{A \times \text{duration}}\right) \quad (3)$$

$$\text{Nitrate yield} = \left(\frac{\text{nitrate loading}}{A \times \text{duration}}\right) \quad (4)$$

where A and duration are catchment area (m^2) and event flow duration (day).

2.4. Nitrate source appointment

To quantify nitrate source contribution, Stable Isotope Analysis in R language (SIAR) uses a Bayesian mixing model to calculate contribution from endmembers (Parnell et al., 2010). This modeling can consider more than two sources and incorporate a fractionation effect (Li et al., 2019; Parnell et al., 2010; Xue et al., 2012). Four potential endmembers from the study area were collected during the study period and analyzed to determine their isotopic composition. To determine soil organic nitrogen (SON), four samples were collected at 0–30 cm depth from four different land uses in July 2017, including farmland, abandoned farmland, grass and shrub land, and forest ($N = 16$). Values for wet deposition (WD, $N = 10$) were identified from research undertaken during the same study period (in May to July 2017) (Zeng et al., 2020). Six synthetic fertilizers (SF) were collected in the study area. To obtain dual nitrate isotopic signature of manure and sewage waste (M&S), water samples were collected five times from a large paddy field within 10 days after application of M&S.

To reduce the uncertainty in our calculations, the isotopic fractionation during the denitrification process was considered in the modeling. The isotopic fractionation of denitrification was obtained from the slope of the relationship between dual nitrate isotopes and ln (NO_3^-) (Eq. (5)). Detailed information regarding Bayesian isotopic mixing modeling (Stable Isotope Analysis in R, SIAR), is provided in the Text S1.1.

2.5. The isotopic fractionation of denitrification

The fractionation of denitrification was calculated using the Rayleigh fractionation method:

$$\delta_r = \delta_0 + \varepsilon \ln(f) \quad (5)$$

where δ_r is the $\delta^{15}N$ or $\delta^{18}O$ value of the residual nitrate which is also the observed $\delta^{15}N$ or $\delta^{18}O$ values, δ_0 is the initial $\delta^{15}N$ or $\delta^{18}O$ value of nitrate, f is the remaining fraction of nitrate, and ε is the isotopic fractionation value (Heffernan et al., 2012; Kendall et al., 2007). To calculate the extent of denitrification (1-f), the high nitrate concentration and low $\delta^{15}N$ or $\delta^{18}O$ value at the beginning of period was used as the initial isotopic composition (δ_0).

3. Results

3.1. Hydrology varies with rainfall

The catchment experienced typical low rainfall and dry conditions before the study (November to the following April 2017, dry season). During the study, the gradual increase in rainfall intensity and periods of concentrated rainfall changed this catchment from dry to wet conditions, and agricultural activity, e.g. tillage, fertilizer application, occurred as normal (Yue et al., 2019). To consider carefully how catchment water storage influences nitrate ex-

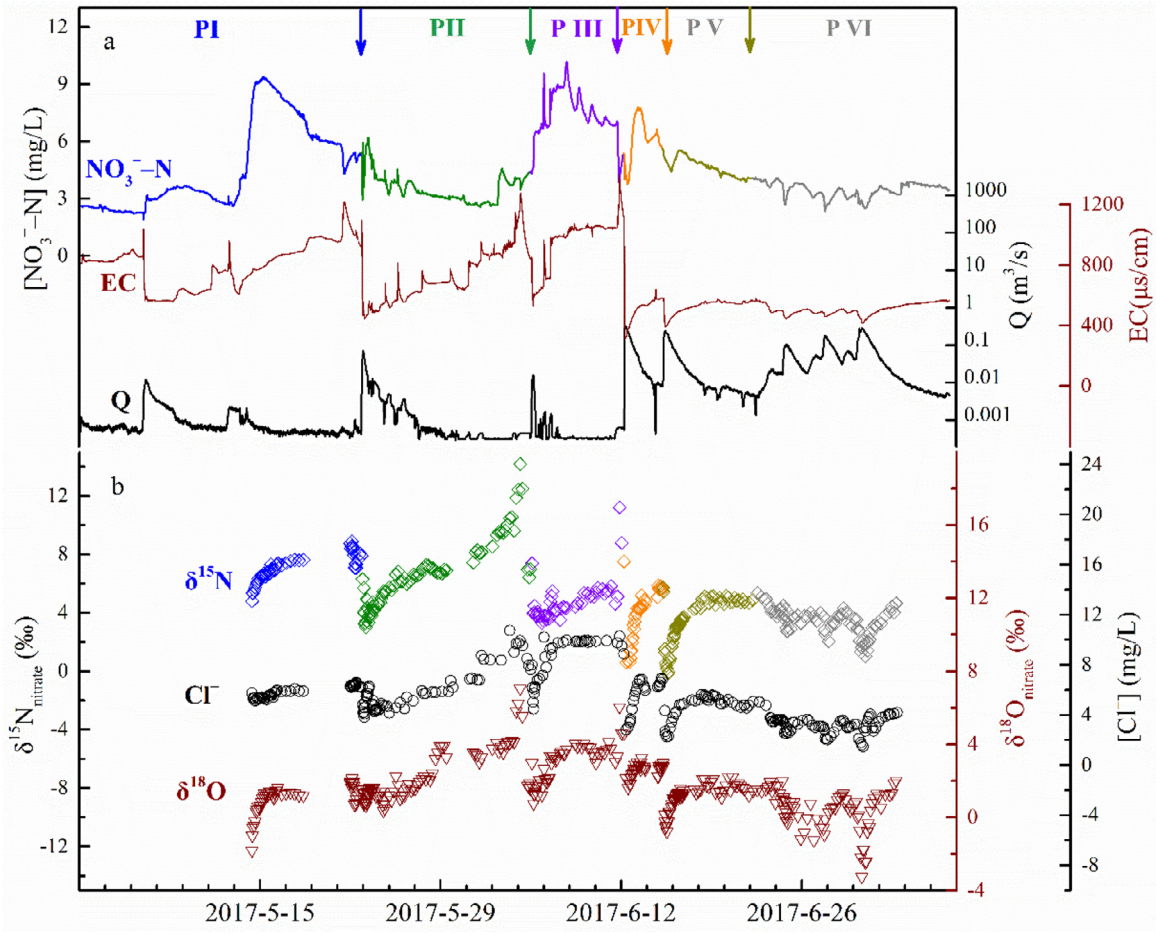

Fig. 2. (a) temporal variation of EC, [NO_3^-–N] and discharge (Q) (Yue et al., 2019); (b) temporal variation of nitrate dual isotopes and [Cl^-] in CHQ catchment. Six different time periods of response are identified, and these are differentiated by different colors.

Table 1
Summary of rainfall (RF), duration (Dur), water level (WL), Temperature (T), discharge (Q), EC and DO in each period.

	RF	Dur	WL	T	Q	EC	DO
	mm	day	m	°C	× 10^{-3} m^3/s	μs/cm	mg/L
Period I	56.3	21.9	$2.73^{3.09}_{2.63} \pm 0.10$	$16.7^{17.8}_{16.3} \pm 0.3$	$1.1^{12.2}_{0.34} \pm 1.5$	$801^{1219}_{559} \pm 148$	$3.2^{4.6}_{2.1} \pm 0.7$ [a]
Period II	40.8	13.1	$3.19^{5.11}_{2.67} \pm 0.26$	$18.0^{22.3}_{16.5} \pm 1.7$	$2.7^{72}_{0.3} \pm 7.7$	$723^{1274}_{446} \pm 170$	$4.8^{10.3}_{0.5} \pm 1.6$
Period III	47.8	7.4	$3.18^{3.39}_{3.12} \pm 0.03$	$20.3^{23.7}_{16.9} \pm 2.1$	$0.8^{15.9}_{0.3} \pm 2.0$	$967^{1393}_{528} \pm 164$	$4.5^{8.3}_{0.4} \pm 1.3$
Period IV	79.4	3.0	$5.18^{7.02}_{3.15} \pm 1.15$	$17.2^{18.2}_{17.0} \pm 0.2$	$65^{332}_{0.4} \pm 85.5$	$521^{1112}_{312} \pm 116$	$5.9^{7.3}_{1.4} \pm 0.9$
Period V	38.8	7.0	$4.33^{6.97}_{3.29} \pm 1.25$	$17.1^{17.4}_{17.0} \pm 0.1$	$30^{242}_{2.3} \pm 50.7$	$527^{581}_{391} \pm 42$	$5.6^{7.1}_{4.9} \pm 0.5$
Period VI	133.6	15.3	$4.91^{7.26}_{3.28} \pm 1.29$	$17.2^{18.0}_{16.9} \pm 0.1$	$46.4^{291}_{1.3} \pm 55.2$	$509^{579}_{414} \pm 36$	$5.9^{7.0}_{5.1} \pm 0.5$

port dynamics, the field data was separated into six short periods (Periods I –VI, PI – VI) based on the time series of Q and water level (WL) at a borehole well (W3 in Chen et al. (2018)) (Fig. 2 & S1). The last three periods were the wet period, constituting 37.4% of the research duration, but with 63.5% of the rainfall recharge. The isotope sampling campaign captured the transition from dry to wet conditions, apparent in changes in Q (Fig. 2).

Scattered rainfall showers occurred frequently and at least one intensive rainfall event (more than 20 mm within 24 h) occurred in each period, causing the discharge to rise, particularly in PIV (74.5 mm/24 h). Although all periods experienced similar rainfall between each period, the water yield can vary by more than eighty times. For example, water yield during PI and PIII ranged from 0.054 to 0.186 mm/day, whereas water yield during PIV and PVI ranged from 2.07 to 4.5 mm/day (Table 1), which suggests that these periods can be separated into 'transitional periods' (PI –PIII) and 'wet periods' (PIV – PVI).

3.2. Time series of [NO_3^-–N] and hydrochemistry

Hydrochemical summaries for each period can be found in Table 1 and Table 2. The [NO_3^-–N] fluctuated considerably, ranging from 1.9 to 10.1 mg/L with a mean of 4.5 mg/L (Table 2). During transitional periods, the first short duration rainfall only produced a small concentration increase (Fig. 2a) while after that a small increase in Q produced an initial maximum [NO_3^-–N] (9.4 mg/L). Subsequently in PI, [NO_3^-–N] slowly decreased over a prolonged period (7 Days). [NO_3^-–N] progressively declined during PII and the range in [NO_3^-–N] was much smaller than in PI. Although there was a relatively small increase to discharge in PIII, [NO_3^-–N] increased to 10.1 mg/L and stayed at similar concentrations until discharge increased in PIV in response to increased rainfall.

Compared to transitional periods (PI-III), [NO_3^-–N] in wet periods have a lower range over successive rainfall events. [NO_3^-–N] maxima were progressively lower at equal or lower Q and showed

Table 2
Summary of [NO_3^-–N], water and nitrate yield, [Cl^-] and dual nitrate isotopes (Mean $^{max}_{min}$ ± SD) for each period identified in Fig. 2.

Periods (number of samples)	NO_3^-–N	Water yield	Nitrate yield	Cl^-	$\delta^{15}N$	$\delta^{18}O$
	mg/L	mm/day	kg/km^2/day	mg/L	‰	‰
Period I (50)	$4.6\ ^{9.4}_{1.9} \pm 2.2$	0.074	0.28	$5.8\ ^{6.6}_{5.1} \pm 0.4$	$7.1\ ^{8.9}_{4.8} \pm 0.9$	$1.1\ ^{2.1}_{-1.8} \pm 0.8$
Period II (80)	$3.5\ ^{6.1}_{2.6} \pm 0.7$	0.186	0.82	$6.0\ ^{10.7}_{3.8} \pm 1.7$	$6.5\ ^{14.2}_{3.0} \pm 2.4$	$2.3\ ^{7.0}_{0.3} \pm 1.4$
Period III (47)	$7.3\ ^{10.2}_{3.8} \pm 1.3$	0.054	0.34	$8.6\ ^{10.3}_{4.5} \pm 1.7$	$4.8\ ^{11.2}_{3.3} \pm 1.4$	$3.0\ ^{6.0}_{0.8} \pm 1.1$
Period IV (36)	$6.2\ ^{7.8}_{3.7} \pm 1.1$	4.5	23.6	$5.7\ ^{8.9}_{2.8} \pm 1.5$	$4.0\ ^{7.5}_{0.6} \pm 1.8$	$2.6\ ^{4.6}_{1.6} \pm 0.5$
Period V (61)	$4.6\ ^{5.6}_{3.9} \pm 0.5$	2.07	10.2	$4.6\ ^{5.6}_{2.3} \pm 1.0$	$3.4\ ^{5.7}_{-0.2} \pm 1.6$	$1.2\ ^{3.0}_{-0.8} \pm 0.8$
Period VI (73)	$3.5\ ^{4.1}_{2.3} \pm 0.4$	3.27	9.9	$3.2\ ^{5.0}_{1.5} \pm 0.7$	$3.4\ ^{5.3}_{1.0} \pm 0.9$	$0.4\ ^{2.0}_{-3.2} \pm 1.1$

relatively stable concentrations of around 3.5 mg/L in PVI. Further, a smaller amplitude of change in [NO_3^-–N] was observed during the falling limb of the hydrograph during wet periods than during transitional periods.

During rainfall events, [NO_3^-–N] increased after an initial dilution at the beginning of events (Fig. 2). Given the short duration of rising limbs of the hydrograph responses in this KCZ, there were no cases whereby maximum [NO_3^-–N] was earlier than maximum Q, indicating that nitrate was being diluted during all rainfall events (except the first one) and as discharge decreased [NO_3^-–N] on the receding limb increased. Similar trends were observed in [Cl^-] and EC (Figs. 2 and S2, Table 2). High fluctuations and the highest values of DO, T and EC were all observed in transitional periods (Tables 1 and 2), particularly T during PII (Table 1).

3.3. The isotopic composition of nitrate in the KCZ

In general, as Q increases, dual nitrate isotopic composition decreases (Fig. 3), with this relationship strongest in the wet periods. Nitrate isotopic compositions were dynamic, ranging from −0.2 to 14.2‰ for $\delta^{15}N$ and from −3.2 to 7.0‰ for $\delta^{18}O$. The range in nitrate isotopic compositions also varied in the six periods, with much variation in PII and PIII (Table 2). The greatest dual isotope values were all observed in PII, whereas the lowest dual isotope values were found during rainfall events in different periods: PV for $\delta^{15}N$ and PVI for $\delta^{18}O$.

3.4. Nitrate source proportions under various hydrological conditions during rainfall events

NO_3^- originating from WD has $\delta^{18}O_{nitrate}$ of more than 60‰ and low $\delta^{15}N_{nitrate}$, which can distinguish this source from other NO_3^- produced by microbial nitrification (Zeng et al., 2020). The isotopic compositions of four dominant endmembers collected from the study area during study periods (Table S1), were used in the SIAR modeling (Fig. 4). The nitrate isotopic composition during the latter stages of PII and in PIII was likely influenced by denitrification and so the corresponding isotopic fractionation was accommodated in the SIAR model for those time periods.

The SIAR modeling showed that contribution of the four nitrate sources varied dynamically during the study period. Wet deposition only contributed 10.5% (MPE) of nitrate export from the catchment in transitional periods and its contribution decreased during wet periods. Although there are large rainfall events (Figs. 2a & 4a) during wet periods, the highest contribution only occurred during PIII when gradually increasing hydrological connectivity facilitated unprocessed atmospheric nitrate export to the outlet. SF contribution during wet periods is higher than SON and M&S, particularly during event flows (with the MPE up to 79.8%). The contribution of SON is relatively constant during the entire study period (about 32%), but decreases during rainfall events. M&S contributed proportionally more nitrate during base flow than event flows, but its contribution varied more during wet periods than transitional periods (Fig. 4d).

SF contribution in wet periods increased with the amount of discharge, and this source exhibited a significant positive relationship ($p < 0.0001$) with Q, which is unlike the SON ($p < 0.0001$) and M&S ($p < 0.0001$) proportional contributions that exhibited a significant negative relationship with Q (Fig. 5). There was no significant relationship between WD and Q suggesting that this source may not be hydrologically controlled in this high [NO_3^-–N] catchment.

The source contributions are shown proportionally and are calculated based on isotopic signature. Total N-nitrate of each source exported from the catchment is calculated through scaling-up to total load by considering the volume of water discharged. For example, SIAR modeling shows that SF was proportionally the largest contribution, at 42 ± 12% (Table S2). However, SF export constituted more, at 54.2% of total nitrate export. Nitrate export from SF was 2.2, 3.4 and 10.1 times greater than SON, M&S, and WD respectively, based on MPE and Q calculations (Table S2, Figure S4).

4. Discussion

4.1. Nitrate export under various hydrological conditions in the KCZ

The rapid response of WL or Q is typical of karst aquifers (Hartmann et al., 2014; Opsahl et al., 2017). The occurrence of two rainfall events and increased water level at the borehole well (W3, Fig. 1) in PII suggested water recharge into the karst aquifer. The relatively stable WL during PIII indicated that the recharge and discharge water from the catchment are balanced, nitrate is being flushed out the system. The rainfall during transitional periods only produced a slight fluctuation of WL and a small amount of discharge water (Fig. 2a) but higher [NO_3^-–N] than wet periods, indicating that rainfall events can initiate further nitrate loss by flushing (Mueller et al., 2016). The slow decrease in [NO_3^-–N] during the transitional period indicated nitrate was transferred in a relatively small amount of water via baseflow.

The highest WL and Q occurred in PVI and PIV, respectively, suggesting that accumulated water during transitional periods, and new recharged water into the karst aquifer system during wet periods, increased the WL leading to more water being discharged from the catchment with high Q during wet periods. Although [NO_3^-–N] was diluted by the successive rainfall events during the wet period, the high Q yielded 1–2 orders of greater nitrate export than the transitional periods, indicating active catchment nitrate mobilization (Table 2).

4.2. The transformations of nitrate under various hydrological conditions in the KCZ

The observed higher $\delta^{18}O$-NO_3^- and high simultaneous $\delta^{15}N$-NO_3^- during the latter stages of PII and PIII and gradual decrease in $\delta^{18}O$-NO_3^- values during wet periods suggested major nitrogen biogeochemistry processes during different periods were varied, such as denitrification and nitrification. Generally, denitrification is likely to occur when there is high moisture in the soil layer

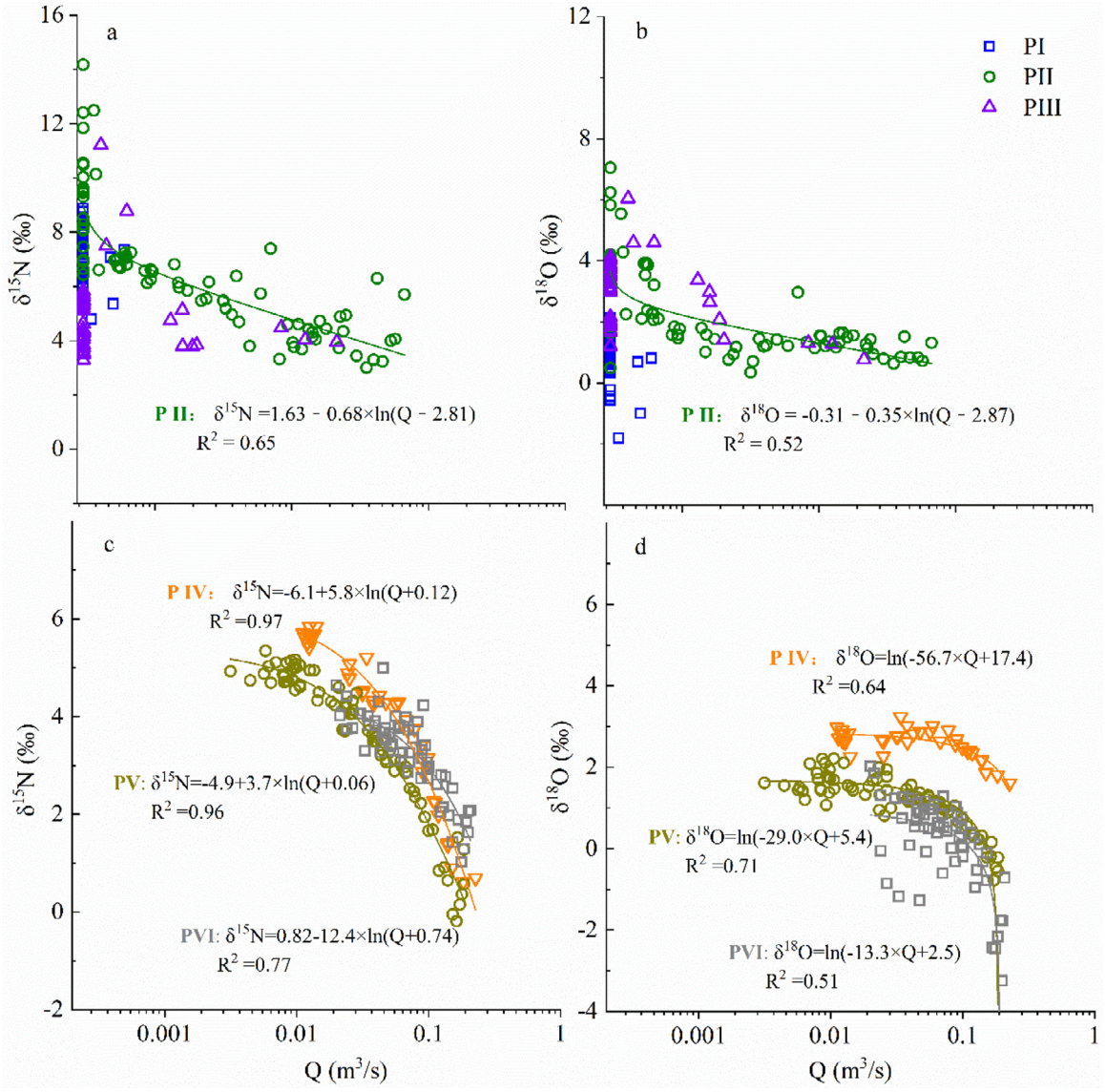

Fig. 3. The relationship between Q and dual nitrate isotopes during transitional periods (a and b) and wet periods (c and d). The colors represent the periods identified in Fig. 2.

(Friedl et al., 2016), and is therefore considered unlikely to occur in the present study during transitional conditions with low moisture. However, PII and PIII were major periods for tillage of paddy fields, which means that farmland would be submerged for rice planting and water residence time would be longer. Thus, the applied N sources and ammonium absorption on the surface soil will be transformed by microbes to nitrate which can be leached to the karst matrix by vertical drainage (Fu et al., 2015; Hattori et al., 2019; Sebestyen et al., 2008). Anaerobic conditions, inferred from low DO concentrations during PII and PIII (Table 1), would occur in the submerged fields to favor denitrification. Thus, the observed higher $\delta^{18}O\text{-}NO_3^-$ and high simultaneous $\delta^{15}N\text{-}NO_3^-$ during the latter stages of PII (slope: 0.6, $p < 0.0001$) and PIII (slope: 0.4, $p < 0.05$) suggest that the increased dual nitrate isotopic composition is driven by denitrification (as modelled in Fig. 6a), which can result in increased $\delta^{15}N$: $\delta^{18}O$ ratios of 2:1, instead of specific sources with enriched ^{15}N or ^{18}O, e.g. M&S and WD (Granger et al., 2008; Kendall et al., 2007). The denitrification of nitrate in karst conduits has previously been observed, using nitrate isotopes and numerical modeling, to occur at higher rates than in groundwater pathways (Husic et al., 2020). Based on the Rayleigh fractionation model ($\delta^{15}N$ & $\delta^{18}O_{nitrate}$ vs. ln (NO_3^-–N) in Fig. 6 b), the extent of denitrification during the later stages of PII and PIII was calculated (Section 2.5) to range from 2.7% to 57.4%, with a mean value 23.9%. This extent of denitrification is smaller than recorded at another karstic aquifer, where a mean value of 32% denitrification was reported in the study of 61 springs (Heffernan et al., 2012).

The minimum $\delta^{15}N\text{-}NO_3^-$ value during PIV and PV showed similar isotopic values (0.6‰ and −0.2‰, respectively) to SF (Table S1), which suggests rapid nitrification (see Text S1.2 for isotope systematic explanation of nitrification) as soil became wetter, completely nitrifying NH_4^+ to nitrate (Quan et al., 2016). Additionally, the high nitrate yield during wet periods and the low concentration of NH_4^+ (89% samples less than 0.1 mg/L) also supports the isotopic interpretation of complete nitrification after PIII. Therefore, the fractionation effect of nitrification for SF is unlikely observed or negligible in the present study. As the catchment progressively became wetter after PIII, nitrified nitrate in soil was more likely to be transported from the source areas, reducing the residence time in KCZ, and thus isotopic composition of nitrate at the spring outlet would be similar to the original endmember and can be used as an endmember of the nitrification signature in SIAR modeling.

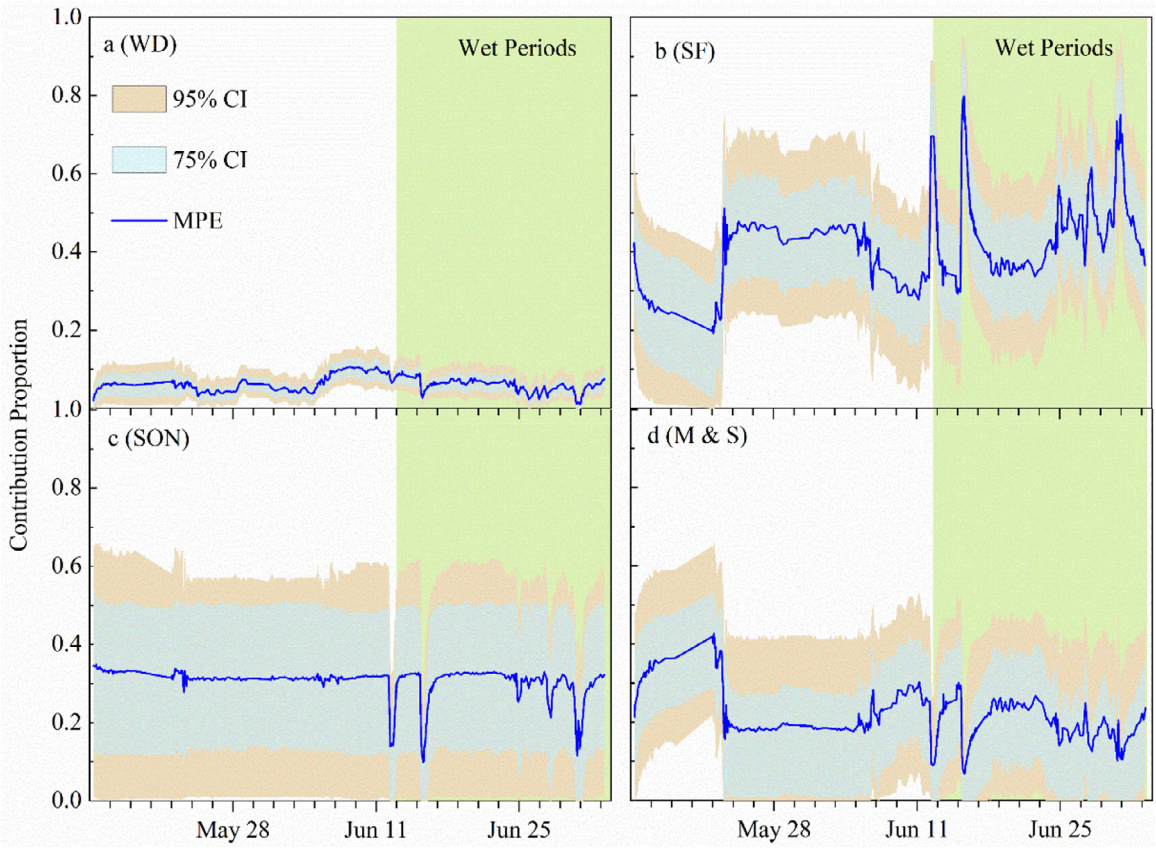

Fig. 4. High resolution source proportional contribution from four sources (a) WD, wet deposition, (b) SF, synthetic fertiliser, (c) SON, soil organic nitrogen and (d) M&S, manure and sewage waste. The mean proportional estimate (MPE) and 75 & 95% confident intervals (CI) are shown.

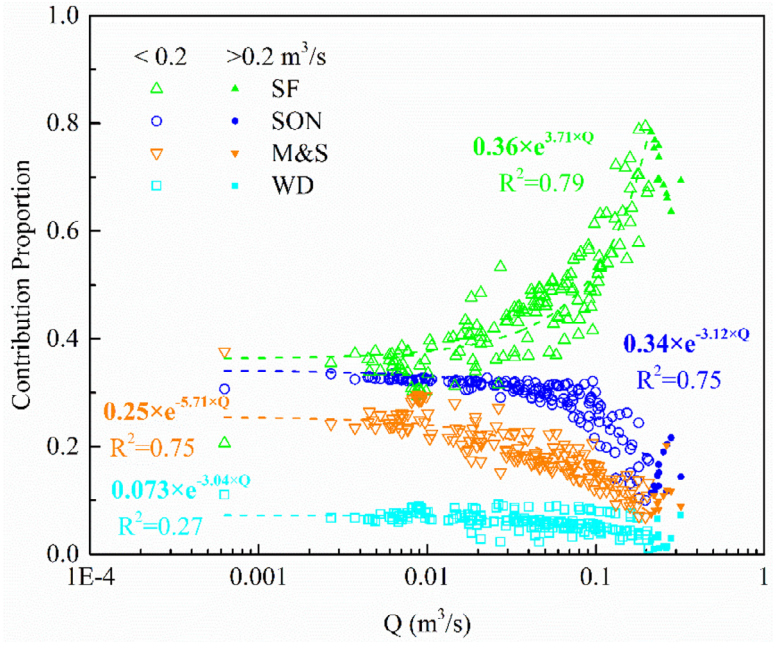

Fig. 5. The relationship between source contribution and Q during wet periods.

The gradual decrease in the $\delta^{18}O\text{-}NO_3^-$ values during wet periods displayed a similar trend to decreasing $\delta^{18}O\text{-}H_2O$ after PIII (Chen et al., 2018), which indicates that the exported nitrate used oxygen atoms from water during nitrification. Although we did not measure $\delta^{18}O\text{-}H_2O$ in transitional periods, the reported range of $\delta^{18}O\text{-}H_2O$ between PIV and VI is from −10.6‰ to −5.1‰, similar to the range in $\delta^{18}O\text{-}H_2O$ (−9.1‰ to 5.8‰) in our previous monthly samples from Houzhai catchment, which includes the present study area (Chen et al., 2018; Yue et al., 2018). Therefore, the reported range of $\delta^{18}O\text{-}H_2O$ between PIV and VI is represen-

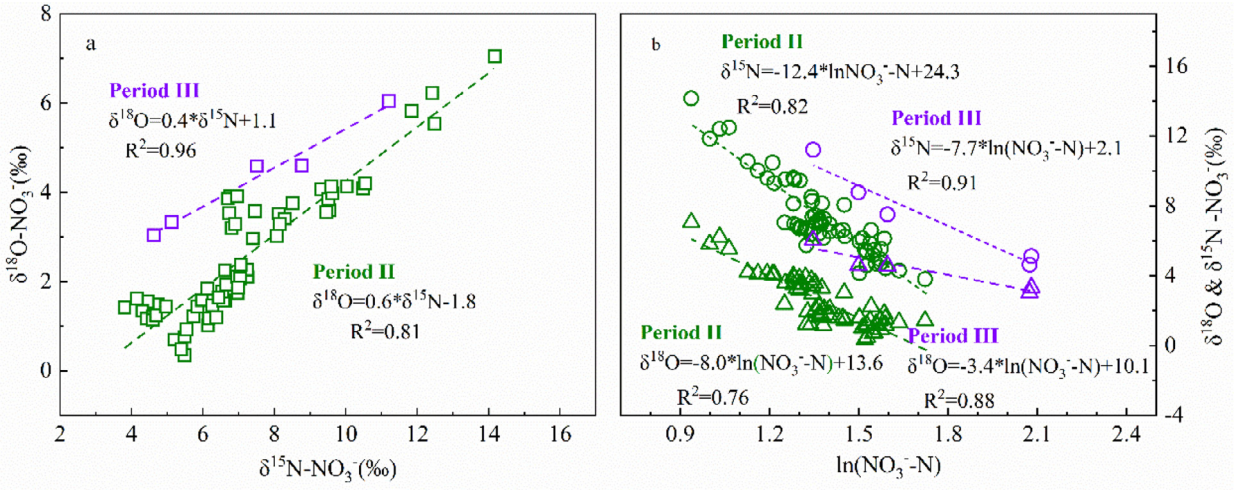

Fig. 6. (a) the relationship of dual nitrate isotopes and (b) fractionation of denitrification of dual nitrate isotopes during later of Period II and III.

tative of the water isotopic composition of the catchment. From the new recent convention ($\delta^{18}O\text{-}NO_3^- = 0.93 \times \delta^{18}O\text{-}H_2O + 2$) (Boshers et al., 2019), the predicted range of $\delta^{18}O\text{-}NO_3^-$ would be −7.9‰ to −2.7‰, which is lower than most of the sample data.

Drainage of tilled land disrupting the clay base would also be evident from increases in EC from higher dissolved solute concentrations (arising from weathering of rock fragments and submerged farmland). The highest EC values in the later stages of PII and PIII are contemporaneous with the increase in dual nitrate isotopes. Therefore, agriculture activities impact on nitrate transformation and hydrochemistry in KCZ, particularly during transitional periods.

4.3. Dynamics of nitrate export controlled by nitrate storage pool of KCZ and hydrology

SIAR modeling demonstrated that nitrate contribution from WD is higher than other large watersheds (Li et al., 2019; Liu et al., 2013) but lower than forested catchments (Sebestyen et al., 2019; Tsunogai et al., 2014). It is interesting that SON contributions remain relatively stable while there are high fluctuations in SF contributions due to rainfall events. The typical geomorphology of peak clusters in the study area and land use (Fig. 1) could facilitate different nitrate pools. Anthropogenic sources such as SF and M&S would be more likely on dry land and paddy fields. SF was typically used for both, whereas M&S was mainly used for paddy fields to improve feed quality due to the decreased number of livestock (Yu et al., 2016). Valley areas with paddy fields and transitional areas with dry land are 'nitrate-rich' due to anthropogenic inputs, e.g. fertilizer application (Green et al., 2019). Hillslope areas with forest or shrub represent the major 'nitrate-limited' areas with most nitrate from WD due to limited anthropogenic N inputs and thin soil layers (Osaka et al., 2016). Therefore, [NO_3^-–N] behavior during events should depend on flushed source areas (Sebestyen et al., 2008). The interaction of spatial variation in source area nitrate loading and transport time, rainfall intensity, distance between source areas to the catchment outlet, and hydrological connectivity (i.e. the nature of pathways and their efficiency in hydrological transport) will interact to control loading to the underground flow (Husic et al., 2019b; Vaughan et al., 2017). Irrespective of which nitrate pool is mobilised, most water will flow through the soil layer (a proportion will bypass the soil matrix via structural cracks) and lead to SON providing a continuous contribution.

4.3.1. Localized flow pathways and nitrate mobilization drive nitrate patterns during transitional periods

During transitional periods, surface soils on hillslopes were not connected to the stream via shallow subsurface flow paths during low rainfall events (Chen et al., 2018; Huebsch et al., 2014). During low intensity rainfall events, NO_3^- flushed in the initial flow should be local (Blaen et al., 2017), e.g. from the valleys. Paddy field areas, which are the major land use in valleys, therefore control the majority of nitrate mobilization. However, a contribution from hillslope or transitional areas cannot be excluded (Jencso et al., 2010): the antecedent accumulated nitrate would also leach from the soil layer and shallow groundwater with high NO_3^- concentrations to the karst matrix and be exported from the catchment outlet. This scenario is more similar to the transitional periods, PI - PIII.

Normally, karst springs have more constant water T than surface water, observed with T in wet periods (Figure S1). However, the progressively increased water T at outlet from 16.3 °C in PI to 23.7 °C in PIII suggested the exported water at the outlet was more likely from surface or subsurface sources as water through soils or karst matrix carries sensible heat. High fluctuations (diurnal variation) in DO also suggested water recharge from surface water as recharge is the only source of DO supply to aquifers. In addition, EC also increased at the same time. Fluctuations of hydrochemistry parameters mainly reflects recharge water within the catchment, e.g. from paddy fields, and also indicates low water storage during these periods. Agricultural irrigation from sinkholes will reduce the water supply from the hillslope areas to the outlet, and reduce the dilution effect from the hillslope area water with low [NO_3^-–N], e.g. among PI and PIII. This resulted in accumulated nitrate in the local area around the outlet in valley areas being leached - observed in PIII with no water level response to rainfall and high [NO_3^-–N] (Fig. 2). The high [NO_3^-–N] and denitrified nitrate during transitional periods all indicated that nitrate originates from a 'nitrate-rich' zone in the valley area around the outlet.

4.3.2. Recharge water from hillslope dilute [NO_3^-–N] during wet periods

When the rainfall intensity increases, the hydraulic connectivity within recharge areas would increase and so connection with stored nitrate (Chen et al., 2018; Vaughan et al., 2017), increasing nitrate mobilization from transitional or hillslope areas depending on the rainfall intensity. Valley or transitional areas may result in more variation in nitrate loading and isotopic signature than hillslope areas with low nitrate availability, and the resultant nitrate

pool would reflect the mixing from these areas. Consequently, nitrate concentration and isotopic composition during wet periods was less variable than in low intensity rainfall events, e.g. PI-PIII.

Hydrological studies of this karst area have identified that heavy rainfall events in hillslope areas lead to a dual flow contribution (Fu et al., 2015; Peng and Wang, 2012), with the majority of flow driven by vertical transfer to the karst aquifer system, which can in turn activate the conduit flow system (Husic et al., 2019b). Additionally, horizontal flow by subsurface or overland flow transfers water to transitional or valley bottom areas to leach the 'nitrate-rich' pool again (Zhang et al., 2019). The active conduit flow from hillslope areas transfers low [NO_3^-–N] water to the outlet more quickly than water from the agricultural areas (high [NO_3^-–N]) due to the thin vadose zone (Zhang et al., 2019). Therefore, the conduit flow or sinkholes (fast flow) with low [NO_3^-–N] contributed more during the rising limb, with later nitrate mobilised and vertically leached to the karstic aquifer network during the falling limb. High [NO_3^-–N] reflects mobilised transitional zone (e.g. dry land) nitrate export by slow flow. The persistent rising water level and discharge showed that new water was entering conduits, fractures, fissures, and the matrix (e.g. during PIV, Figure S1). This also explained why peak [NO_3^-–N] lagged peak discharge: an increased contribution by slow flow causing high [NO_3^-–N] in the falling limb.

High Q did not always correspond to high MPE of SF (solid symbols, Fig. 5). Fig. 5 indicates that the maxima Q of events (12th, 15th and 30th June during wet periods) corresponded to some characteristics of nitrate from base flow, which means this originated from the stored nitrate in the karst matrix or soil layer (e.g. Husic et al., 2019b). Although the accumulated nitrate pool in soil may not be fully leached during transitional periods, there should be little available after two heavy events (12th and 15th) in contrast to the high nitrate yield in the wet periods. For example, the sharp increase in water yield and NO_3^- yield during PIV suggested that a large proportion of the nitrified NO_3^- stored in the surface soil was flushed out during heavy rainfall events occurring in wet periods (e.g. Blaen et al., 2017; Sebestyen et al., 2019). The progressively increasing water yield and NO_3^- yield suggested transport of a large pool of accumulated NO_3^- in KCZ, particularly from the agricultural areas of the valley depressions. This is more obvious in PV. Despite rainfall in PV being lower than the following high rainfall event (79.4 mm) in PIV, a high-water yield and NO_3^- yield occurred in PV indicating that discharged water and nitrate came from antecedent storage. The significant relationship between source contribution and discharge indicated that hydrologically controlled patterns of nitrogen leaching in karst areas are more dependent on anthropogenic nitrogen, e.g. SF and M&S. Wet periods are important to hydrologically connect the export channels among nitrate source zones, which has also been reported in the karst aquifer system of central Texas (Musgrove et al., 2016). However, it is still unclear whether intense rainfall during one event or successive rainfall events is the strongest influence on hydrological connectivity in this KCZ. With the frequency of rainfall events expected to increase as a result of climate change (IPCC, 2014), there is a need to manage karst agroecosystems more carefully to minimize nutrient loss from land and fluvial contamination.

5. Conclusion

This research highlights how dual nitrate isotopes can provide depth of understanding of high resolution [NO_3^-–N] time series in karst aquifer system. With these tools we can identify the dominant sources of nitrate and how they change with time, we can infer how nitrate is reprocessed, stored and transported in the high heterogeneous KCZ, and we can quantify the load exported of each source. Our results supported our hypothesis that spatial storage of nitrate and the extent to which these zones are connected with hydrological flow pathways in the karst influences the nitrate loading in emergent waters. The low rainfall events stored NO_3^- in KCZ, while high rainfall events accelerated nitrate export, particularly nitrate from SF. With such understanding we can support the development of land management practices, particularly the timing of fertilization to avoid application during successive rainfall periods.

Declaration of Competing Interest

The authors declare that they have no known competing financial interests or personal relationships that could have appeared to influence the work reported in this paper.

Acknowledgments

The authors would like to acknowledge funding from the National Natural Science Foundation of China, Grant/Award Number: 41571130072 and the UK Natural Environment Research Council, Grant/Award Number: NE/N007425/1. Sensor and hydrochemistry data for this site and others from these grants can be found at https://doi.org/10.5285/f70596a1-0994-4b08-abab-0c9398af447d. We thank Drs. Jie Zeng, Cai-Qing Qin, Yu-Chong Fu for their help in sampling collection. In addition, we would like to thank the Puding Karst Ecosystem Research Station for providing rainfall data. F-JY, S-LL, SW and DO designed the research objectives and interpreted the data and prepared the manuscript. F-JY and Z-JW carried out the field and laboratory work. F-JY, C-QL and S-LL conducted data analysis. XC aided the hydrological interpretation and interpreted the hydrological knowledge. All of authors participated in discussion of the results.

Supplementary materials

Supplementary material associated with this article can be found, in the online version, at doi:10.1016/j.watres.2020.116388.

Reference

Banwart, S., Chorover, J., Gaillardet, J., Sparks, D., White, T., Anderson, S., Aufdenkampe, A., Bernasconi, S., Brantley, S., Chadwick, O., 2013. Sustaining Earth's critical Zone Basic Science and Interdisciplinary Solutions For Global Challenges. University of Sheffield, Sheffield, UK, p. 47.

Blaen, P.J., Khamis, K., Lloyd, C., Comer-Warner, S., Ciocca, F., Thomas, R.M., MacKenzie, A.R., Krause, S., 2017. High-frequency monitoring of catchment nutrient exports reveals highly variable storm event responses and dynamic source zone activation. J Geophys Res-Biogeo 122 (9), 2265–2281.

Boshers, D.S., Granger, J., Tobias, C.R., Böhlke, J.K., Smith, R.L., 2019. Constraining the Oxygen Isotopic Composition of Nitrate Produced by Nitrification. Environ Sci Technol 53 (3), 1206–1216.

Brantley, S., White, T.S., White, A.F., Sparks, D., Richter, D., Pregitzer, K., Derry, L., Chorover, J., Chadwick, O., April, R., Anderson, S. and Amundson, R.2006Frontiers in Exploration of the Critical Zone: report of a workshop sponsored by the National Science Foundation (NSF), Newark.

Chen, X., Zhang, Z.C., Soulsby, C., Cheng, Q.B., Binley, A., Jiang, R., Tao, M., 2018. Characterizing the heterogeneity of karst critical zone and its hydrological function: an integrated approach. Hydrol Process 32 (19), 2932–2946.

Cui, S.H., Shi, Y.L., Groffman, P.M., Schlesinger, W.H., Zhu, Y.G., 2013. Centennial-scale analysis of the creation and fate of reactive nitrogen in China (1910-2010). P Natl Acad Sci USA 110 (6), 2052–2057.

Epting, J., Page, R.M., Auckenthaler, A., Huggenberger, P., 2018. Process-based monitoring and modeling of Karst springs - Linking intrinsic to specific vulnerability. Sci Total Environ 625, 403–415.

Ford, D., Williams, P.D., 2013. Karst Hydrogeology and Geomorphology. John Wiley & Sons.

Ford, W.I., Husic, A., Fogle, A., Taraba, J., 2019. Long-term assessment of nutrient flow pathway dynamics and in-stream fate in a temperate karst agroecosystem watershed. Hydrol Process 33 (11), 1610–1628.

Friedl, J., Scheer, C., Rowlings, D.W., McIntosh, H.V., Strazzabosco, A., Warner, D.I., Grace, P.R., 2016. Denitrification losses from an intensively managed sub-tropical pasture–Impact of soil moisture on the partitioning of N2 and N2O emissions. Soil Biology and Biochemistry 92, 58–66.

Fu, T.G., Chen, H.S., Zhang, W., Nie, Y.P., Wang, K.L., 2015. Vertical distribution of soil saturated hydraulic conductivity and its influencing factors in a small karst catchment in Southwest China. Environ Monit Assess 187 (3), 92.
Gooddy, D.C., Lapworth, D.J., Bennett, S.A., Heaton, T.H., Williams, P.J., Surridge, B.W., 2016. A multi-stable isotope framework to understand eutrophication in aquatic ecosystems. Water Res 88, 623–633.
Granger, J., Sigman, D.M., Lehmann, M.F., Tortell, P.D., 2008. Nitrogen and oxygen isotope fractionation during dissimilatory nitrate reduction by denitrifying bacteria. Limnol. Oceanogr. 53 (6), 2533–2545.
Green, S.M., Dungait, J.A., Tu, C., Buss, H.L., Sanderson, N., Hawkes, S.J., Xing, K., Yue, F., Hussey, V.L. and Peng, J. 2019. Soil functions and ecosystem services research in the Chinese karst Critical Zone. Chem Geol.
Gu, B.J., Ju, X.T., Chang, J., Ge, Y., Vitousek, P.M., 2015. Integrated reactive nitrogen budgets and future trends in China. P Natl Acad Sci USA 112 (28), 8792–8797.
Hartmann, A., Goldscheider, N., Wagener, T., Lange, J., Weiler, M., 2014. Karst water resources in a changing world: review of hydrological modeling approaches. Rev Geophys 52 (3), 218–242.
Hattori, S., Nuñez Palma, Y., Itoh, Y., Kawasaki, M., Fujihara, Y., Takase, K., Yoshida, N., 2019. Isotopic evidence for seasonality of microbial internal nitrogen cycles in a temperate forested catchment with heavy snowfall. Sci Total Environ 690, 290–299.
Heffernan, J.B., Albertin, A.R., Fork, M.L., Katz, B.G., Cohen, M.J., 2012. Denitrification and inference of nitrogen sources in the karstic Floridan Aquifer. Biogeosciences 9 (5), 1671–1690.
Hu, M.P., Liu, Y.M., Zhang, Y.F., Dahlgren, R.A., Chen, D.J., 2019. Coupling stable isotopes and water chemistry to assess the role of hydrological and biogeochemical processes on riverine nitrogen sources. Water Res 150, 418–430.
Huebsch, M., Fenton, O., Horan, B., Hennessy, D., Richards, K.G., Jordan, P., Goldscheider, N., Butscher, C., Blum, P., 2014. Mobilisation or dilution? Nitrate response of karst springs to high rainfall events. Hydrol. Earth Syst. Sci 18 (11), 4423–4435.
Husic, A., Fox, J., Adams, E., Backus, J., Pollock, E., Ford, W., Agouridis, C., 2019a. Inland impacts of atmospheric river and tropical cyclone extremes on nitrate transport and stable isotope measurements. Environ Earth Sci 78 (1), 36.
Husic, A., Fox, J., Adams, E., Ford, W., Agouridis, C., Currens, J., Backus, J., 2019b. Nitrate Pathways, Processes, and Timing in an Agricultural Karst System: development and Application of a Numerical Model. Water Resour Res 55 (3), 2079–2103.
Husic, A., Fox, J., Adams, E., Pollock, E., Ford, W., Agouridis, C., Backus, J., 2020. Quantification of nitrate fate in a karst conduit using stable isotopes and numerical modeling. Water Res 170, 115348.
IPCC, 2014. Climate change 2014: synthesis report. In: Contribution of Working Groups I, II and III to the Fifth Assessment Report of the Intergovernmental Panel On Climate Change. IPCC, Geneva, Switzerland, p. 151.
Jarvie, H.P., Sharpley, A.N., Kresse, T., Hays, P.D., Williams, R.J., King, S.M., Berry, L.G., 2018. Coupling High-Frequency Stream Metabolism and Nutrient Monitoring to Explore Biogeochemical Controls on Downstream Nitrate Delivery. Environ Sci Technol 52 (23), 13708–13717.
Jencso, K.G., McGlynn, B.L., Gooseff, M.N., Bencala, K.E., Wondzell, S.M., 2010. Hillslope hydrologic connectivity controls riparian groundwater turnover: implications of catchment structure for riparian buffering and stream water sources. Water Resour Res 46 (10), W10524.
Jiang, Y.J., Wu, Y.X., Yuan, D.X., 2009. Human Impacts on Karst Groundwater Contamination Deduced by Coupled Nitrogen with Strontium Isotopes in the Nandong Underground River System in Yunan, China. Environ Sci Technol 43 (20), 7676–7683.
Kendall, C., Elliott, E.M. and Wankel, S.D. 2007. Tracing anthropogenic inputs of nitrogen to ecosystems. Stable Isotopes in Ecology and Environmental Science, 375–449.
Kordilla, J., Sauter, M., Reimann, T., Geyer, T., 2012. Simulation of saturated and unsaturated flow in karst systems at catchment scale using a double continuum approach. Hydrol Earth Syst Sc 16 (10), 3909–3923.
Li, C., Li, S.-.L., Yue, F.-.J., Liu, J., Zhong, J., Yan, Z.-.F., Zhang, R.-.C., Wang, Z.-.J., Xu, S., 2019. Identification of sources and transformations of nitrate in the Xijiang River using nitrate isotopes and Bayesian model. Sci Total Environ 646, 801–810.
Liu, T., Wang, F., Michalski, G., Xia, X., Liu, S., 2013. Using ^{15}N, ^{17}O, and ^{18}O To determine nitrate sources in the Yellow River, China. Environ Sci Technol 47 (23), 13412–13421.
Luo, W., Xu, X.L., Liu, W., Liu, M.X., Li, Z.W., Peng, T., Xu, C.H., Zhang, Y.H., Zhang, R.F., 2019. UAV based soil moisture remote sensing in a karst mountainous catchment. Catena 174, 478–489.
McIlvin, M.R., Casciotti, K.L., 2011. Technical Updates to the Bacterial Method for Nitrate Isotopic Analyses. Anal. Chem. 83 (5), 1850–1856.
Mueller, C., Zink, M., Samaniego, L., Krieg, R., Merz, R., Rode, M., Knoller, K., 2016. Discharge Driven Nitrogen Dynamics in a Mesoscale River Basin As Constrained by Stable Isotope Patterns. Environ Sci Technol 50 (17), 9187–9196.
Musgrove, M., Opsahl, S.P., Mahler, B.J., Herrington, C., Sample, T.L., Banta, J.R., 2016. Source, variability, and transformation of nitrate in a regional karst aquifer: edwards aquifer, central Texas. Sci Total Environ 568, 457–469.
Opsahl, S.P., Musgrove, M., Slattery, R.N., 2017. New insights into nitrate dynamics in a karst groundwater system gained from in situ high-frequency optical sensor measurements. J Hydrol 546, 179–188.
Osaka, K., Kugo, T., Komaki, N., Nakamura, T., Nishida, K., Nagafuchi, O., 2016. Atmospheric nitrate leached from small forested watersheds during rainfall events: processes and quantitative evaluation. J Geophys Res-Biogeo 121 (8), 2030–2048.
Parnell, A.C., Inger, R., Bearhop, S., Jackson, A.L., 2010. Source Partitioning Using Stable Isotopes: coping with Too Much Variation. PLoS ONE 5 (3), e9672.
Peng, T., Wang, S.J., 2012. Effects of land use, land cover and rainfall regimes on the surface runoff and soil loss on karst slopes in southwest China. Catena 90, 53–62.
Pu, J.B., Yuan, D.X., He, Q.F., Wang, Z.J., Hu, Z.Y., Gou, P.F., 2011. High-resolution monitoring of nitrate variations in a typical subterranean karst stream, Chongqing, China. Environ Earth Sci 64 (7), 1985–1993.
Quan, Z., Huang, B., Lu, C.Y., Shi, Y., Chen, X., Zhang, H.Y., Fang, Y.T., 2016. The fate of fertilizer nitrogen in a high nitrate accumulated agricultural soil. Sci Rep-Uk 6, 21539.
Sebestyen, S.D., Boyer, E.W., Shanley, J.B., Kendall, C., Doctor, D.H., Aiken, G.R., Ohte, N., 2008. Sources, transformations, and hydrological processes that control stream nitrate and dissolved organic matter concentrations during snowmelt in an upland forest. Water Resour Res 44 (12), W12410..
Sebestyen, S.D., Ross, D.S., Shanley, J.B., Elliott, E.M., Kendall, C., Campbell, J.L., Dail, D.B., Fernandez, I.J., Goodale, C.L., Lawrence, G.B., Lovett, G.M., McHale, P.J., Mitchell, M.J., Nelson, S.J., Shattuck, M.D., Wickman, T.R., Barnes, R.T., Bostic, J.T., Buda, A.R., Burns, D.A., Eshleman, K.N., Finlay, J.C., Nelson, D.M., Ohte, N., Pardo, L.H., Rose, L.A., Sabo, R.D., Schiff, S.L., Spoelstra, J., Williard, K.W.J., 2019. Unprocessed Atmospheric Nitrate in Waters of the Northern Forest Region in the U.S. and Canada. Environ Sci Technol 53 (7), 3620–3633.
Sullivan, P.L., Macpherson, G.L., Martin, J.B., Price, R.M., 2019. Evolution of carbonate and karst critical zones. Chem Geol. 527, 119223.
Tsunogai, U., Komatsu, D.D., Ohyama, T., Suzuki, A., Nakagawa, F., Noguchi, I., Takagi, K., Nomura, M., Fukuzawa, K., Shibata, H., 2014. Quantifying the effects of clear-cutting and strip-cutting on nitrate dynamics in a forested watershed using triple oxygen isotopes as tracers. Biogeosciences 11 (19), 5411–5424.
Vaughan, M.C.H., Bowden, W.B., Shanley, J.B., Vermilyea, A., Sleeper, R., Gold, A.J., Pradhanang, S.M., Inamdar, S.P., Levia, D.F., Andres, A.S., Birgand, F., Schroth, A.W., 2017. High-frequency dissolved organic carbon and nitrate measurements reveal differences in storm hysteresis and loading in relation to land cover and seasonality. Water Resour Res 53 (7), 5345–5363.
Wong, C.I., Mahler, B.J., Musgrove, M., Banner, J.L., 2012. Changes in sources and storage in a karst aquifer during a transition from drought to wet conditions. J Hydrol 468, 159–172.
Xue, D., De Baets, B., Van Cleemput, O., Hennessy, C., Berglund, M., Boeckx, P., 2012. Use of a Bayesian isotope mixing model to estimate proportional contributions of multiple nitrate sources in surface water. Environ Pollut 161, 43–49.
Yang, X., Jomaa, S., Büttner, O., Rode, M., 2019. Autotrophic nitrate uptake in river networks: a modeling approach using continuous high-frequency data. Water Res 157, 258–268.
Yu, G., Ran, W. and Shen, Q. (2016) From Basic Concepts to Applied Outcomes, Soloneski, M.L.L.a.S. (ed), IntechOpen.
Yue, F.-.J., Li, S.-.L., Zhong, J., Liu, J., 2018. Evaluation of Factors Driving Seasonal Nitrate Variations in Surface and Underground Systems of a Karst Catchment. Vadose Zone J 17 (1).
Yue, F.-.J., Waldron, S., Li, S.-.L., Wang, Z.-.J., Zeng, J., Xu, S., Zhang, Z.-.C., Oliver, D.M., 2019. Land use interacts with changes in catchment hydrology to generate chronic nitrate pollution in karst waters and strong seasonality in excess nitrate export. Sci Total Environ 696, 134062.
Yue, F.-.J., Waldron, S., Oliver, D. and Ding, H. 2020 Hydrochemistry and nitrate sensor data from three karst sites in SW China, 2016–2017. Centre, N.E.I.D. (ed).
Zeng, J., Yue, F.-.J., Li, S.-.L., Wang, Z.-.J., Qin, C.-.Q., Wu, Q.-.X., Xu, S., 2020. Agriculture driven nitrogen wet deposition in a karst catchment in southwest China. Agric Ecosyst Environ 294, 106883.
Zhang, X., Davidson, E.A., Mauzerall, D.L., Searchinger, T.D., Dumas, P., Shen, Y., 2015. Managing nitrogen for sustainable development. Nature 528 (7580), 51.
Zhang, Z.C., Chen, X., Cheng, Q.B., Soulsby, C., 2019. Storage dynamics, hydrological connectivity and flux ages in a karst catchment: conceptual modelling using stable isotopes. Hydrol Earth Syst Sc 23 (1), 51–71.